Continuum limit of amorphous elastic bodies. III. Three-dimensional systems

F. Leonforte,[1,*] R. Boissière,[1] A. Tanguy,[1] J. P. Wittmer,[2] and J.-L. Barrat[1]
[1]*Laboratoire de Physique de la Matière Condensée et des Nanostructures, Université Claude Bernard (Lyon I) and CNRS, 43 Boulevard du 11 Novembre 1918, 69622 Villeurbanne Cedex, France*
[2]*Institut Charles Sadron, CNRS, 6, Rue Boussingault, 67083 Strasbourg, France*
(Received 25 May 2005; revised manuscript received 21 October 2005; published 15 December 2005)

Extending recent numerical studies on two-dimensional amorphous bodies, we characterize the approach of the elastic continuum limit in three-dimensional (weakly polydisperse) Lennard-Jones systems. While performing a systematic finite-size analysis (for two different quench protocols), we investigate the nonaffine displacement field under external strain, the linear response to an external δ force, and the low-frequency harmonic eigenmodes and their density distribution. Qualitatively similar behavior is found as in two dimensions: The classical elasticity description breaks down below a surprisingly large length scale ξ, which in our system is approximately 23 molecular sizes. This length characterizes the correlations of the nonaffine displacement field, the self-averaging of external noise with distance from the source, and gives the lower wavelength bound for the applicability of the classical eigenfrequency calculations. Moreover, we demonstrate that the position of the "Boson peak" in the density of vibrational states is related to this self-averaging length ξ.

DOI: 10.1103/PhysRevB.72.224206 PACS number(s): 46.25.−y, 72.80.Ng, 83.80.Fg

I. INTRODUCTION

In a recent series of papers,[1–3] we investigated the elastic response of zero-temperature two-dimensional (2D) amorphous systems. Our studies were motivated by the idea that such systems, although they appear perfectly homogeneous when looking at the density field, may be described as heterogeneous from the point of view of the theory of elasticity. The basic reason for this failure is now well identified: the underlying *hypothesis of affinity* of elastic deformations, implicit in standard elastic theory,[4,5] need not apply to a disordered system. The relevant issue is therefore the scale above which a disordered, glassy system can be considered as homogeneous from an elastic point of view.

Obviously, this question is important for the vibrational spectrum of such disordered systems; the excess of vibrational states at intermediate frequencies in the spectrum (the so-called Boson peak) has previously been assigned to the existence of elastic heterogeneities,[6,7] whose existence appears to be confirmed by recent experiments.[8] Moreover, the field of *plastic* deformation of glassy materials, which has attracted considerable attention recently,[9–14] may be expected to be related to elastic heterogeneities. Other points of interest include the experimental evidence for dynamical heterogeneities in deeply supercooled systems,[15] which again could be expected to give rise to "frozen-in" heterogeneities in low-temperature systems.

Our previous studies were limited to 2D systems, as this reduced dimension allows one to carry out calculations on systems with large linear box sizes L using a limited number of particles. These studies allowed us to establish, for a standard computational model system, the existence of a length scale ξ that can reach a few tens of particles, and below which classical elasticity breaks down. Similar conclusions were reached by Goldhirsch and Goldenberg.[16] This breakdown is revealed by a number of different diagnostics: (i) The so-called Born expression for elastic constants is found to give incorrect results. This failure can be traced back to the importance of a nonaffine contribution to the microscopic displacement field, while the derivation of the Born formula assumes affine displacement at all scales. The analysis of the correlation function of the nonaffine contribution to the displacement field reveals ξ as the distance over which this field is correlated, defining "soft" regions with large nonaffine displacements. (ii) The study of low-frequency vibrations in these model disordered systems shows that the predictions of classical elastic theory are recovered only for wavelengths larger than ξ, meaning the system is not homogeneous from the point of view of elastic properties below this scale. (iii) More recently, it was shown that the response to a point force is dominated by fluctuations for distances to the source smaller than ξ.[3] Hence, ξ characterizes the self-averaging of the noisy response within each configuration, which led us to call it the *self-averaging length*. (iv) The influence of pressure has been investigated in two dimensions, demonstrating that ξ remains "mesoscopic" for low and moderate pressures, typically of the order of 40 particle sizes, but decreases at large pressures.[17]

An obvious question that arises is the extent to which these results may depend, qualitatively or quantitatively, on the *dimensionality of space*. Three-dimensional (3D) systems, however, are considerably more difficult to study than the 2D case. The limit of elastically homogeneous systems requires lateral system sizes L much larger than ξ. Supposing ξ to be comparable to what is observed in two dimensions imposes an order of at least 10^5 particles to be considered, if one wants to use the same tools and diagnostics in 2D and 3D systems. Although a number of studies have appeared recently[18–20] pointing to the existence of elastic inhomogeneities in various types of disordered systems, all of them were realized for relatively small system sizes, making a direct comparison to our previous results difficult. In the same way, previous calculations of vibration modes in 3D systems have been limited to rather small sizes.[21–23] This work explores systems with lateral sizes that are appreciably larger than the expected scale of elastic heterogeneities.

The aim of this work is therefore to characterize the elastic behavior of large 3D systems, using the same computer model and similar quench protocols as in our previous 2D studies, and to explore possible relations between the nonaffine mechanical response and the excess of vibrational states—the so-called Boson peak. System parameters and quench protocols are summarized in Sec. II. In Sec. III, we begin by analyzing the nonaffine local displacement field in cubic samples submitted to uniaxial elastic deformation. From previous experience,[1,2] we know that this type of analysis is the most cost effective in revealing the existence of inhomogeneities and their length scale. We then discuss the elastic response to a point force (Sec. IV) and corroborate why ξ has been termed "self-averaging length." Vibrational properties at very low eigenfrequencies—obtained by diagonalization of the dynamical matrix—are considered in Sec. V and the density of eigenstates—computed by means of the finite temperature velocity autocorrelation function—is considered in Sec. VI. Our results are summarized in Sec. VII.

II. DESCRIPTION OF SYSTEMS AND SIMULATION PROCEDURES

The initial configurations and their preparation are deliberately similar to those described in Ref. 1 for the 2D case. The same slightly polydisperse Lennard-Jones potential $U_{ij}(r)=4\epsilon\,[(\sigma_{ij}/r)^{12}-(\sigma_{ij}/r)^{6}]$ has been used with σ_{ij} uniformly distributed between 0.8σ and 1.2σ. The corresponding polydispersity index 0.12 is expected to be enough to destabilize a polydisperse crystal,[24] and indeed no sign of crystallization or demixing was observed in our simulations.[25] The interaction energy scale ϵ and the particle masses m will be taken to be strictly monodisperse. In the following, we will adopt Lennard-Jones units, i.e., the mean diameter σ will be our unit of length (and generically described as the "particle size"), while time will be expressed in units of $\tau=\sqrt{m\sigma^2/\epsilon}\approx 1$ ps. We studied systems at constant density, $\rho=N/L^3=0.98$, which corresponds for small temperatures to a very low hydrostatic pressure ($|P|\approx 0.2$). The lateral size L of the periodic simulation box was varied between $L=8$ and $L=64$ (corresponding to $N=500$ and $N=256\,000$ particles).

Disordered configurations are prepared by melting at high temperature ($k_BT/\epsilon=2$) an initially fcc configuration during 10^5 molecular dynamics steps (MDS) using standard constant temperature molecular dynamics.[1,25] After the system was equilibrated, we begin the production run using two types of minimization. The first one, called the "fast quench," uses a direct conjugate gradient minimization until (according to numerical tolerance) the zero-temperature equilibrium state is reached. This protocol was implemented for all system sizes. The second "slow quench" protocol has been used only up to $L=40$ ($N=62\,500$). In this case, the liquid configuration is first equilibrated at $k_BT/\epsilon=1$ and then cooled down at stages ($k_BT/\epsilon=5.10^{-1},10^{-1},5.10^{-2},\ldots,10^{-3}$) where the system is "aged" (rather than "equilibrated") during 10^5 MDS.[25] Finally, the zero-temperature state is reached using conjugate gradient minimization. Unless indicated otherwise, all the results refer to ensemble averages (over 10 independent realizations) carried out with the fast quench procedure.

III. RESPONSE TO A MACROSCOPIC UNIAXIAL DEFORMATION

A. Computational procedure and nonaffine displacement fields

In this section, we investigate the elastic behavior of zero-temperature cubic samples, prepared as described above, submitted to an uniaxial traction. The procedure adopted is the following. First, a global deformation of strain $\epsilon_{xx}\ll 1$ is imposed on the sample by rescaling all the coordinates in an *affine* manner, that is $\underline{r}_i^{\mathrm{aff}}=(\underline{\underline{1}}+\underline{\underline{\epsilon}})\underline{r}_i$ where $\underline{r}_i$ stands for the initial position of the particle i and $\underline{r}_i^{\mathrm{aff}}$ is the resulting position. Starting from this affinely deformed configuration (with constant $\underline{\underline{\epsilon}}$), the system is then relaxed to the nearest energy minimum, keeping the shape of the simulation box constant.[25] As a result, a displacement of the particles relative to the affinely deformed state is observed. This defines the *nonaffine* displacement $\underline{u}(\underline{r}_i)$ of each particle i; that is, $\underline{u}(\underline{r}_i)\equiv\underline{r}_i^{f}-\underline{r}_i^{\mathrm{aff}}$, where $\underline{r}_i^{f}$ stands for the final position of the particle i after the relaxation.

A typical example for these displacements in the *linear elastic* response limit (for a strain of $\epsilon_{xx}\approx 10^{-7}$) is presented in the first panel of Fig. 1. It displays the projection of $\underline{u}(\underline{r})$ on a plane containing the elongation direction for a system of size $L=40$. (Note that projections on different planes are similar.) Visual inspection of such snapshots suggests that nonaffine displacements are *strongly* correlated over short and intermediate distances. This impression is also confirmed by Fig. 1(b) where we focus on the 10 % most mobile particles suggesting a connected cluster of these strong displacements spanning the simulation cell. The long-range spatial correlations of these displacements will be discussed below in Sec. III D.

In fact, the nonaffine response depends on the amplitude of the strain imposed. In Fig. 2, we present the first moments $\langle[\underline{u}(\underline{r}_i)]^{2n}\rangle^{1/2n}$ of the nonaffine displacements in a system of size $L=40$, averaged over all particles of an ensemble, as a function of the imposed strain. Both quench protocols give very similar results. (Only one moment is given for the slow protocol for clarity.) For $\epsilon\ll\epsilon_p(L=40)\approx 10^{-6}$ (vertical line), all moments are (up to prefactors of order one) identical, which demonstrates an unique strain dependence for all beads. As one may also expect, a linear strain dependence is found (bold line). At $\epsilon_p(L)$, however, the moments increase suddenly and differ over more than an order of magnitude. This suggests an inhomogeneous strain dependence of the nonaffine displacement field from this value of the imposed strain. This will also be discussed below (Fig. 3). We stress finally that the threshold $\epsilon_p(L)$ decreases extremely rapidly with increasing system size. (A detailed quantitative description is beyond the scope of this study.) Hence, linear response requires much smaller deformations for large L.

B. Plastic displacements and participation ratio

The elastic (reversible) character of the deformations for small ϵ_{xx} is checked by carrying out the reverse transforma-

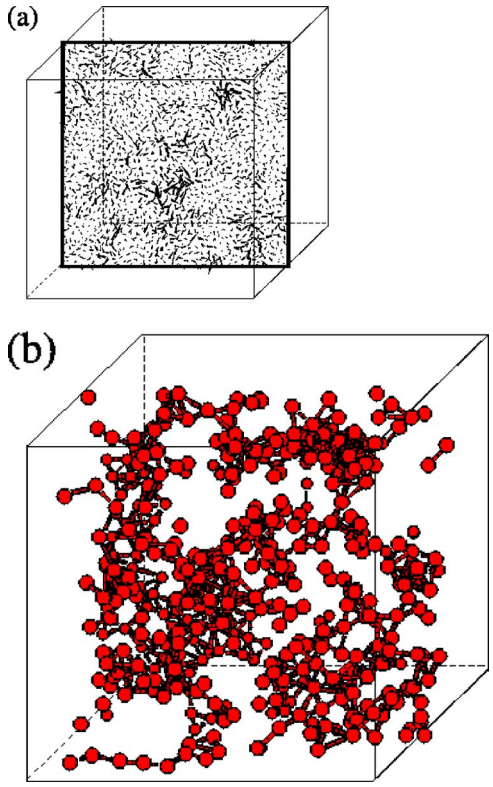

FIG. 1. (Color online) Nonaffine part of the linear and reversible displacements $\underline{u}(\underline{r}_i)$ for the imposed macroscopic uniaxial strain $\epsilon_{xx}=10^{-7}$ for a system containing $N=62\,500$ beads ($L=40$): (a) projection on the $(x-z)$-plane for all particles close to the plane. The length of the arrow is proportional to the displacement. (b) All beads of the same configuration with the 10% strongest nonaffine displacements. (The short lines indicate beads with direct mutual interactions.) This subset of beads is strongly spatially correlated on short distances, however, it is homogeneously distributed and isotropic on larger scales.

tion and measuring the residual displacement of the particles, $\underline{v}_i$, which corresponds to plastic deformation. The moment $\langle \|\underline{v}_i\| \rangle_i$ of the residual displacement is indicated in Fig. 2. For $\epsilon_{xx} \ll \epsilon_p$ it is negligible and the deformation is, hence, elastic. Interestingly, elastic and linear elastic regimes coincide, as can be seen from the figure. For larger strains the residual displacements increase sharply over several orders of magnitude and coincide roughly with the $n=1$ moment of the nonaffine displacements. This shows that, for $\epsilon_{xx} > \epsilon_p$, the nonaffine displacements are mainly due to plastic rearrangements.

In view of the potential relationship with plastic deformation, it is interesting to investigate in some detail the spatial features of the nonaffine displacement field. Qualitatively, this can be achieved by representing, as shown in Fig. 1(b), the particles that have the 10% largest nonaffine displacements. This picture shows that the nonaffine field for $\epsilon_{xx} \ll \epsilon_p$ is rather delocalized, with the cluster formed by the most mobile particles spanning the entire simulation cell. A more quantitative view can be obtained by calculating the participation ratio for the nonaffine displacements, defined by

$$P \equiv \frac{1}{N} \frac{[\sum_i \underline{u}(\underline{r}_i)^2]^2}{\sum_i [\underline{u}(\underline{r}_i)^2]^2}. \tag{1}$$

This participation ratio is shown in Fig. 3 as a function of ϵ_{xx}, for both quench protocols and $L=40$. (A similar participation ratio may be calculated for the *residual* plastic displacements. In this latter case, however, the ratio at small ϵ is due to numerics and at high strain it is identical to the participation ratio of the nonaffine displacements.) Obviously, for sufficiently small deformations the displacements must depend identically for *all* beads on the applied strain and P has to become constant. As anticipated in Fig. 2, the presented data show that this coincides with the linear elastic regime where all moments of the nonaffine displacements are similar and the residual plastic field can be neglected.[26] The central point is here that the plateau value of the participation ratio is large ($\sim 25\ \%$) indicating that the elastic nonaffine displacements involve a substantial fraction of the particles. When the deformation exceeds the plastic threshold ϵ_p, however, the participation ratio falls rapidly, indicating that a plastic deformation proceeds via well-*localized* events.[27] The implication from this difference in behavior is that the localized events occurring in plastic deformation cannot be directly inferred from the general *pattern* of nonaffine displacements. This does not mean that plastic displacements and strong nonaffine elastic displacements are completely uncorrelated. In other words, energy barriers (which are relevant for plastic deformation) are not directly related to the local curvature of the energy minima.[28]

Interestingly, the main influence of performing a slow quench seems to be that the plasticity limit is increased, meaning that the system has been brought to a slightly more stable configuration with higher energy barriers without, apparently, changing measurably the local curvature of the energy minima. In fact, properties such as the vibrational modes discussed below, are much less affected by the quench protocol.

In the reminder of this paper, we thus only focus on the *linear* elastic response. We thus normalize the nonaffine displacements by the second moment, i.e., $\underline{u}(\underline{r}_i)$ is replaced by $\underline{u}(\underline{r}_i)/\langle \underline{u}^2 \rangle^{1/2}$, in order to consider a strain-independent reduced displacement field.

C. Hydrodynamic limit: Lamé coefficients

We turn now to the calculation of the Lamé coefficients λ and μ, which characterize the elastic behavior of an isotropic medium in three dimensions.[5] Our results for these coefficients as a function of system size are shown in Fig. 4, which compares two different ways of obtaining the coefficients. λ_a and μ_a are obtained under the assumption that the nonaffine contribution to the total displacement field of the particles is negligible. They are simply the Born estimates, which can be, in a system with pairwise interactions potential U, computed from the reference configuration by carrying out a simple summation over all pairs of interacting particles (see, for example, Refs. 1 and 9): $\lambda_a=\mu_a=(1/L^3)\Sigma_{i,j}\ [U''(r_{ij}) - (1/r_{ij})U'(r_{ij})]x_{ij}^2 y_{ij}^2/r_{ij}^2$. The second estimate corresponds to

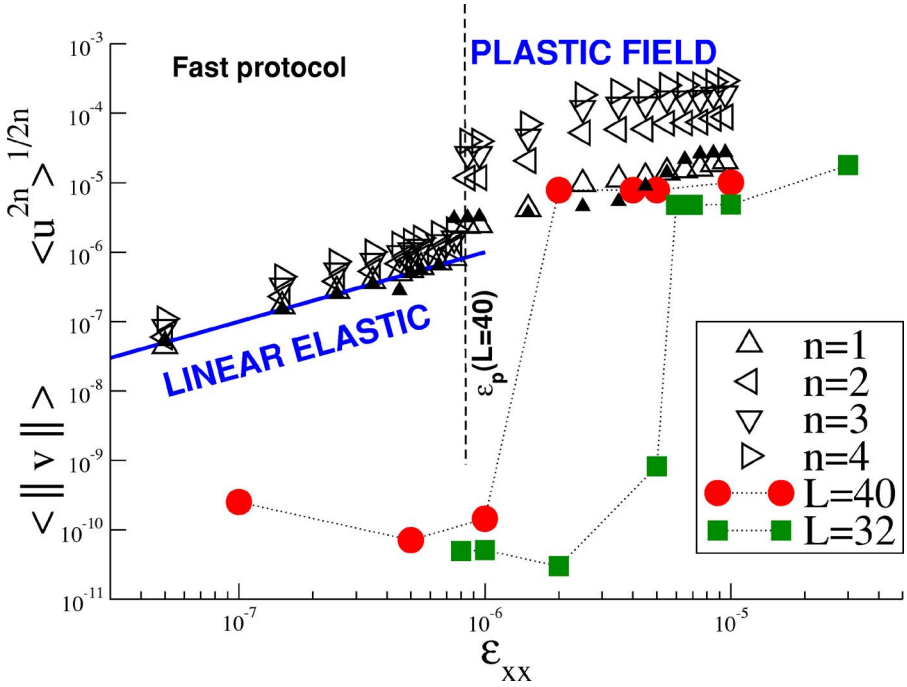

FIG. 2. (Color online) Different moments of nonaffine displacement field $\langle \underline{u}^{2n} \rangle^{1/2n}$ as a function of the imposed strain ϵ_{xx} for systems of $L=40$ obtained by means of the fast (open triangles) and the slow (full triangles) quench protocol. Both protocols show very similar results. The bold line on the left indicates the linear slope $\langle \underline{u}^{2n} \rangle^{1/2n} \propto \epsilon_{xx}$. The vertical dashed line marks the limit of elastic response $\epsilon_p(L) \approx 10^{-6}$ for $L=40$. Also given is the residual plastic displacement field $\langle \| \underline{v} \| \rangle$ (obtained by reverse deformation back to the original macroscopic shape) for $L=40$ and $L=32$ (full symbols). Residual fields below 10^{-9} are due to numerical inaccuracies, and the field can be considered as reversible. The sudden rise at ϵ_p for $L=40$ corresponds nicely to the jump of the moments $\langle \underline{u}^{2n} \rangle^{1/2n}$. Note that the plasticity threshold ϵ_p depends strongly on the system size.

the "true" value of the elastic coefficients, obtained by computing (by means of the usual Kirkwood expression[2]) the incremental stress $\bar{\sigma}_{\alpha\beta}$ (Greek indices referring to cartesian coordinates) *after* the relaxation that introduces the nonaffine part of the displacement field.

The Lamé coefficients are then obtained from the standard formulas $\bar{\sigma}_{xx}=(\lambda+2\mu)\epsilon_{xx}$ and $\bar{\sigma}_{yy}=\lambda\epsilon_{xx}$ for a deformation tensor that has only an ϵ_{xx} component (ϵ_{xx} is here the global deformation imposed on the sample). For larger systems, we obtain $\mu \approx 15$ and $\lambda \approx 47$. Hence, we find that the true values of λ and μ differ considerably from the Born estimates, which indicates the importance of nonaffine displacements in determining the stresses in the material. This contribution tends to lower the shear modulus μ and to increase the co-

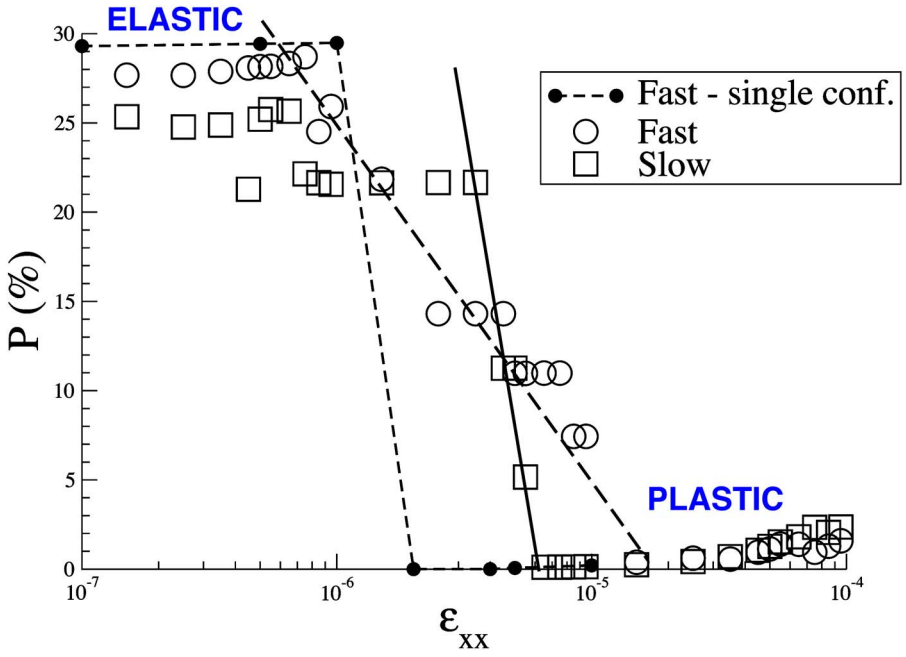

FIG. 3. (Color online) Participation ratio of the nonaffine displacement field in a 3D system containing 62 500 particles ($L=40$), as a function of the uniaxial strain ϵ_{xx} for both fast and slow quench protocols averaged over eight and five configurations, respectively. The given lines are guides to the eye.

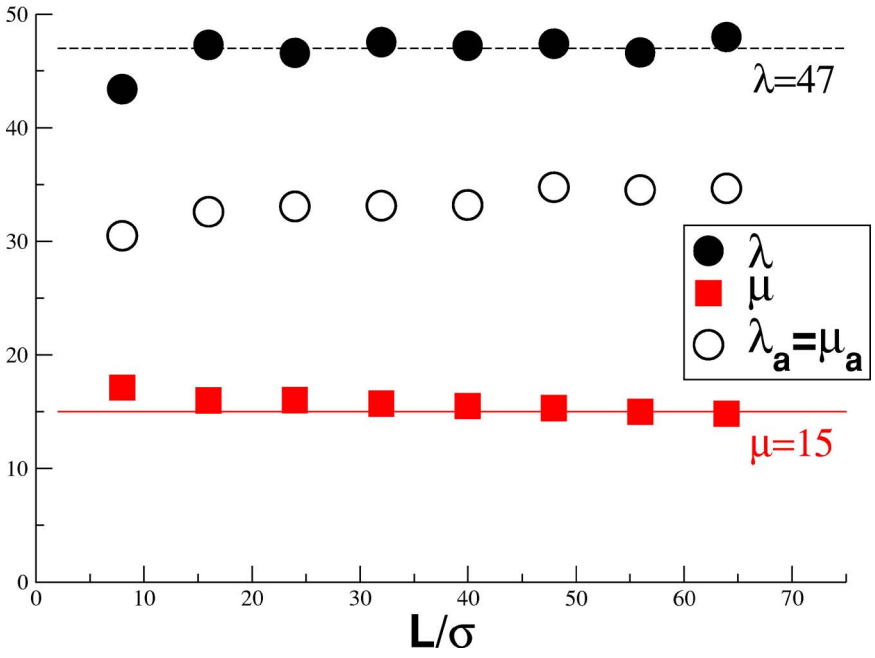

FIG. 4. (Color online) Lamé coefficients λ (spheres) and μ (squares) vs system size L. Full symbols correspond to the direct measurement using Hooke's law; open symbols are obtained supposing *affine* deformations (Born term). The effect of system size is weak. The coefficients relying on a negligible nonaffine field differ by a factor as large as 2 from the true ones. Clearly, a calculation taking into account the nonaffine character of the displacement is necessary for disordered systems.

efficient λ. From the measured values of λ and μ we get a bulk compression modulus $K=\lambda+2\mu/d\approx 57$, a Young's modulus $E=8K\mu/(3K+\mu)\approx 37$, and a Poisson's ratio $\nu=(3K-2\mu)/2(3K+\mu)\approx 0.4$.[5] Remarkably, as well as for 2D systems, the bulk modulus K would be correctly predicted by the Born calculation. This means that the nonaffine part of the deformation does not contribute significantly to the increment in the *isotropic* pressure under compression or traction, but is mainly associated with shear deformations. (The discussion of Fig. 6 below will elucidate this point.) Such a situation would be natural in high-pressure systems, in which the repulsive inverse power part of the potential dominates the interaction and compression can be accommodated by an affine rescaling of all coordinates. It is, however, less expected in our low-pressure systems.

D. Correlations in the nonaffine displacement field

The preceding results call for a more thorough analysis of the correlations of the nonaffine displacement field, which apparently cannot be neglected for macroscopic quantities and should therefore be even more relevant for finite wavelength properties.

Following Refs. 1 and 2, the nonaffine correlation field can be analyzed by computing the correlation function $C(r)\equiv\langle \underline{u}(\underline{r}_i)\underline{u}(\underline{r}_j)\rangle$. [The averages are taken over all pairs of monomers (i,j) being a distance r apart.] As can be seen in Fig. 5(a), a decay over a typical length of 23 particle sizes is observed (bold line), before the correlation function exhibits a *negative* tail. The 2D case included for comparison shows qualitatively similar behavior. The anticorrelation can be associated visually in two dimensions with the solenoidal character of the nonaffine displacement field.[1,2] The organization of the nonaffine deformation in "vortices" is less obvious in three dimensions as manifested by the about-seven-times-weaker amplitude of the negative tail.

That the displacement field is, indeed, correlated over a size $\xi \gg \sigma$ (as indicated by the direct visualization of Fig. 1) is further clarified in Fig. 5(b). Here we consider the systematic coarse graining of the displacement field $\underline{U}_j(b)\equiv 1/N_j\Sigma_{i\in V_j}\underline{u}(\underline{r}_i)$ of all N_j beads contained within the cubic volume element V_j of linear size b.[2] In the figure, we have plotted the (normalized) correlation function $B(b)\equiv[\langle \underline{U}_j(b)^2\rangle_j/\langle \underline{u}^2\rangle]^{1/2}$ versus the size of the coarse-graining volume element b (normalized by L). For both 2D and 3D systems we find an *exponential* decay. It is well fitted by the characteristic scales $\xi\approx 23$ for three dimensions and $\xi\approx 42$ for two dimensions. Apparently, ξ is similar to the distance where $C(r)$ becomes anticorrelated. Note that the total nonaffine displacement field of the box must vanish—since the center of mass of the system is fixed—and therefore $B(b)\to 0$ for $b/L\to 1$. This sum rule explains the curvature in the data and the sharp cutoff on the right-hand side of the figure.

More systematically, the displacement field can also be investigated in Fourier space $\underline{U}(\underline{k})\equiv\Sigma_{i=1}^{N}\underline{u}(\underline{r}_i)\exp(i\underline{k}\underline{r}_i)$, where the wave vectors $\underline{k}$ must be chosen commensurate with the periodic simulation box. Apart the normalization factor $1/N_j$, this is close to the coarse graining of the displacement field over a volume element. We can demonstrate now that the nonaffine displacement field in three dimensions is, indeed, of a predominantly *solenoidal* nature. This has been anticipated by our previous studies on 2D systems[1] and by the values of the elastic moduli μ and K discussed in Sec. III C. More quantitatively, the transverse and longitudinal contributions to the displacement field can be numerically obtained by computing $\underline{T}(\underline{k})\equiv-(1/k^2)\underline{k}\wedge[\underline{k}\wedge\underline{U}(\underline{k})]$ and $\underline{L}(\underline{k})\equiv(1/k^2)\underline{k}[\underline{k}\underline{U}(\underline{k})]$. Obviously, $\underline{U}=\underline{T}+\underline{L}$, $\underline{k}\underline{U}=\underline{k}\underline{L}$, $\underline{k}\wedge\underline{U}=\underline{k}\wedge\underline{T}$ and $\underline{k}\underline{T}=\underline{k}\wedge\underline{L}=0$. The norms of these quantities, for instance,

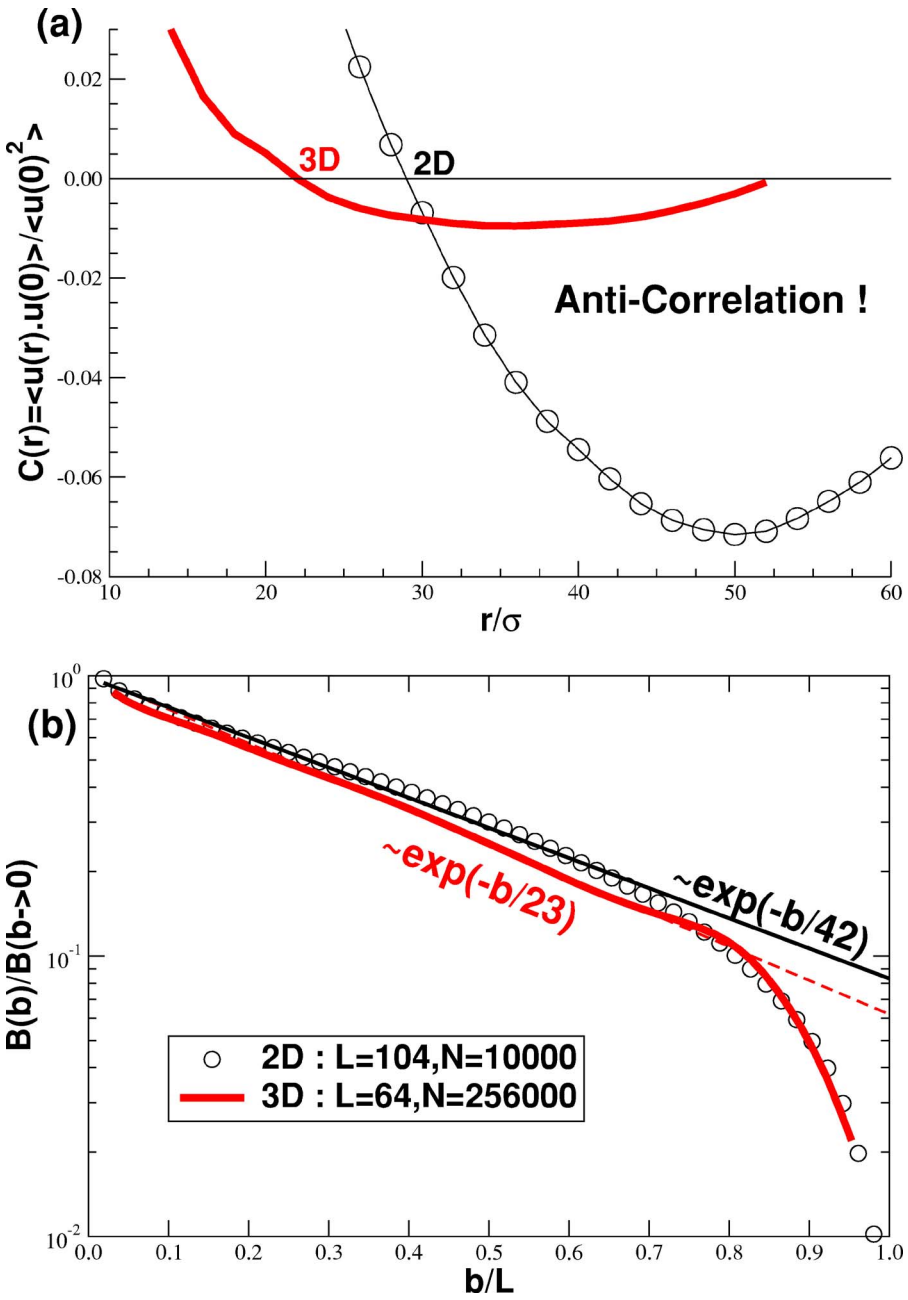

FIG. 5. (Color online) Characterization of the nonaffine deformation field in 2D (open spheres) and 3D (bold lines). The 3D sample corresponds to a system containing 256 000 particles ($L=64$). Note that the "fast" quench protocol and the "slow" quench protocol (not shown here) give identical results. Data from Ref. 1 for a 2D system of linear size $L=104$ is shown for comparison: (a) $C(r)$ as a function of the distance between pairs of beads r. Note the *negative*—although weak—correlation of the 3D correlation function for $r>23\sigma$. (b) The (normalized) magnitude $B(b)$ of the nonaffine field averaged over a volume element of lateral size b is traced as a function of b/L. The correlations decay with a characteristic length $\xi=23$ for 3D and $\xi=42$ for 2D, respectively.

$$k^2 S_T(k) \equiv \frac{k^2}{N}\langle \|\underline{T}(\underline{k})\|^2\rangle = \frac{1}{N}\left\langle \left\| \sum_i \underline{k} \wedge \underline{u}(\underline{r}_i)\exp(i\underline{k}\cdot\underline{r}_i)\right\|^2\right\rangle \tag{2}$$

and similarly for the longitudinal part $k^2 S_L(k)$, are the Fourier transforms of $\nabla \wedge \underline{u}$ and ∇u. They are plotted in Fig. 6 as functions of $\lambda = 2\pi/k$. Note that all data points in this figure, obtained for different system sizes, collapse well for wavelengths corresponding to the nonaffine displacement regime, $\lambda < \xi$. Note that the longitudinal contribution (bottom data) is about 10 times smaller than the transverse one. This corroborates the predominantly solenoidal nature of the reversible nonaffine displacement field. Moreover, we find that $k^2 S_T(k)$ is more or less constant while $k^2 S_L(k)$ decreases weakly. Since $\underline{T}$ and $\underline{L}$ are orthogonal this yields the algebraic relation $1/N\langle \|\underline{U}(\underline{k})\|^2\rangle = S_T(k) + S_L(k) \approx S_T(k) \propto 1/k^2$ for the total fluctuations, and large k. This confirms that spatial correlations are long range.

Unfortunately, for larger λ the statistics deteriorate because of the smaller number of wave vectors that can be considered. Our data may suggest that $S_T(k)$ increases for $\lambda > \xi$; however, new data with larger boxes and with better statistics is warranted to confirm this. The Fourier transform is thus not the best way to determine accurately a characteristic length in this case. However, the three methods compared here give complementary results. They all agree with the existence of long-range correlations in the 3D nonaffine reversible displacement field at small imposed external strain, with a characteristic mesoscopic size ξ.

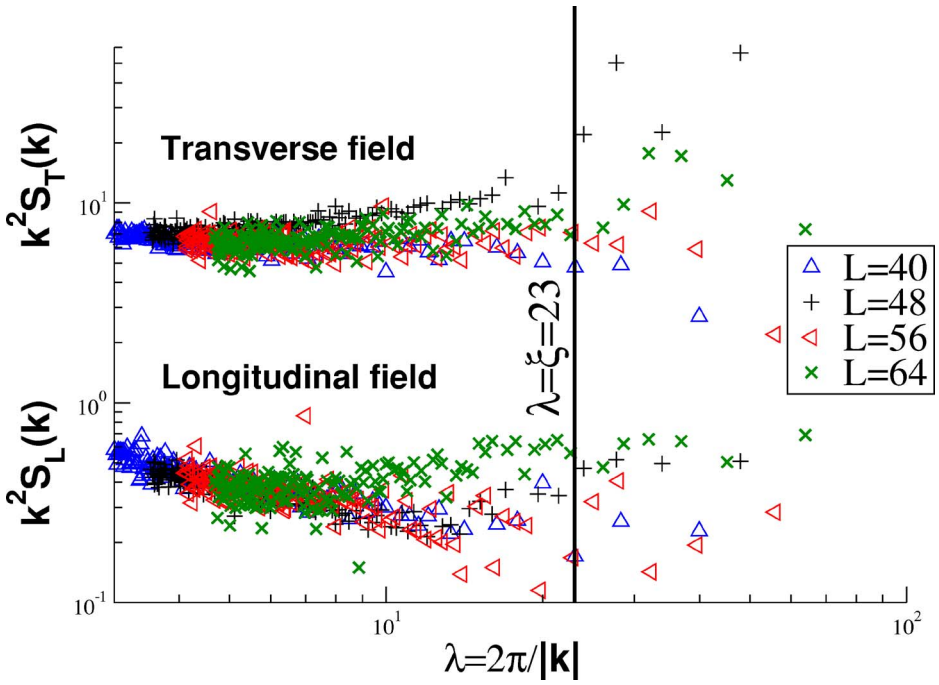

FIG. 6. (Color online) The squared amplitudes of the Fourier transforms k^2S_L and k^2S_T for the div (lower data) and curl (upper data) of the nonaffine deformation field [see Eq. (2)] plotted as functions of the wave length $\lambda=2\pi/\|\underline{k}\|$. Different system sizes have been included to demonstrate that S_L and S_T are system size independent for small λ. Note that the statistics deteriorates for large λ.

IV. SELF-AVERAGING OF THE RESPONSE TO A POINT FORCE

In two dimensions, we showed previously[3] that the deviations from continuum elasticity at small scales could be revealed as well by studying the response of the system to a localized force. The same effect is illustrated for three dimensions in Fig. 7. This plot is obtained as follows. A small force is applied to the particles contained in a small region of space (sphere of diameter 4). The force is applied in the z direction, and its magnitude is chosen small enough to remain in the (linear) elastic region.[25] In order to maintain global force balance, the system has periodic boundary conditions in the x and y directions, but is immobilized by two fixed walls in the z direction. The dimensions of the simulation cell, which contains $N=165\,000$ particles, are $L_z\simeq 105$ in the z direction and $L_x=L_y\simeq 40$ in lateral directions. The Kirkwood stress tensor is then computed for small rectangular boxes of fixed size (3, 3, 5) centered at (x,y,z).[3,16,25] Those boxes are displaced in all the material by unit steps of one in the three directions. For each step, the six components of the stress tensor are calculated and averaged on a statistical ensemble of 200 configurations. Such an ensemble is obtained by taking 10 independent configurations and, for

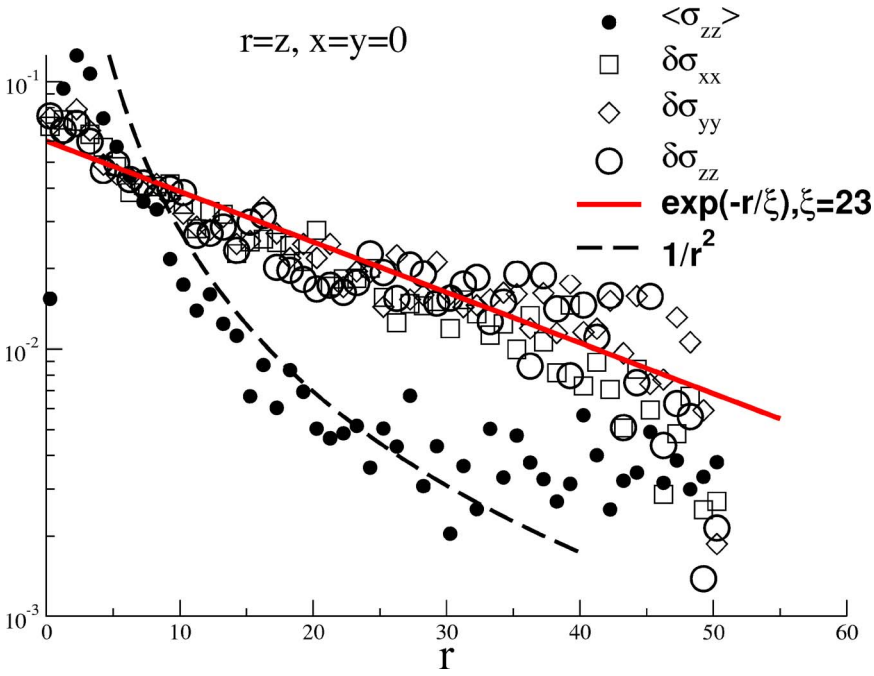

FIG. 7. (Color online) Comparison of the incremental stress fluctuations $\delta\sigma_{\alpha\beta}\equiv(\langle\sigma_{\alpha\beta}^2\rangle-\langle\sigma_{\alpha\beta}\rangle^2)^{1/2}$ with the mean vertical component of normal stress $\langle\sigma_{zz}\rangle$, for volume elements along the vertical line ($r=z$, $x=y=0$). The mean stress decreases essentially as $1/r^2$, as expected (without logarithmic corrections) in three dimensions for positions far from the source and the fixed walls. (Note that $\langle\sigma_{zz}\rangle$ has to decrease less rapidly close to the walls, $r\approx L/2$.) In contrast, the fluctuations decay exponentially over the whole available system. The characteristic length scale is similar to the size $\xi\approx 23\sigma$ of the correlated nonaffine displacements.

each configuration, by changing the position of the point source within the sample, reindexing the configuration in such a way that the origin of the source still is placed in the midplane, equally distant from the two fixed walls. In the absence of the external force, the local stresses in amorphous systems are usually nonzero ("quenched stresses"). The relevant quantity that defines the response to an external force are therefore the *incremental*, rather than total, local stress tensor. Once such a calculation is completed, the quantity of interest is the fluctuations of the incremental stress tensor in the statistical ensemble.[3]

In Fig. 7, both the average value and the fluctuations of the stress tensor are shown. The average response is compared to the prediction of continuum elasticity, which appears to be perfectly obeyed *on average*, even very close to the source. This average response exhibits the $1/r^2$ decay characteristics of the Green's function of classical elasticity in three dimensions. However, up to length scales of 50 the fluctuations are considerably larger than the average value of the stress. The fluctuations, on the other hand, decay *exponentially* away from the source, with a characteristic length 23—the same value as obtained from the correlation functions discussed in Sec. III. In fact, the *relative* stress fluctuations, for instance, $\delta\sigma_{zz}/\langle\sigma_{zz}\rangle$, scale like $\exp(-r/\xi)r^2$ and show nonmonotoneous behavior (not shown). They *increase* first up to 2ξ (due to the decreasing mean stress), but decrease ultimately exponentially. Hence, self-averaging of the noisy signal within each configuration occurs on distances set again by ξ. Unfortunately, our simulation boxes are yet too small to more clearly illustrate the exponential decay of the relative noise for $r \gg 2\xi \approx 50$.

V. LOW-FREQUENCY EQUILIBRIUM VIBRATION MODES

We turn now to the determination of low-frequency vibration modes. These were determined from a direct diagonalization of the dynamical matrix, using a modified version of the PARPACK package.[29] For a periodic cubic system described by classical elasticity, the structure of the low-frequency end of the spectrum is well known. Each mode is characterized by a wave vector $\underline{k}=(2\pi/L)(l,m,n)$. Transverse (longitudinal) have frequencies $\omega=c_T\underline{k}$ (resp. $\omega=c_Lk$), where the sound velocity is given by $c_T=\sqrt{\mu/\rho}\approx 4.2$ (resp. $c_L=\sqrt{(\lambda+2\mu)/\rho}\approx 8.9$). As a result, the modes should have well defined degeneracies. For example, the lowest lying mode $(\pm 1,0,0)$ should have 12-fold degeneracy, corresponding to the two transverse polarizations for the six wave vectors of length $2\pi/L$. The second frequency has degeneracy 24, and so on. In our previous analysis of 2D systems,[1] we found that this degeneracy of the low-frequency modes was lifted for small systems sizes.

Our results for the low-frequency modes of 3D systems are shown in Fig. 8. The plot of the rescaled and averaged frequencies $\langle y\rangle=\langle(\omega L/2\pi c_T)^2\rangle$ as a function of mode number p [Fig. 8(a)] clearly demonstrates that only large systems, containing at least 32 000 particles ($L=32$), show the expected degeneracies and the associated steplike behavior.[30] For the largest systems (lateral size 64), however, the discreteness of the low-frequency spectrum is well apparent, typically up to the fourth eigenfrequencies. In view of the large value of c_L compared to c_T ($c_L\simeq 2.1c_T$ in our system), we have concentrated on the analysis of transverse modes. Longitudinal modes enter only at higher frequencies and are mixed with shorter wavelength transverse modes, making their contribution more difficult to identify. If we take as a criterion the existence of a gap separating the first 12 eigenfrequencies from the rest of the spectrum, it appears that the minimum size for applying continuum elasticity is comprised between $L=16$ and $L=32$.

This analysis can be refined using a scaling plot of the mode frequencies as a function of the "theoretical" wavelength or, more precisely, the wavelength of the elastic wave that would appear in the spectrum with this mode number according to elastic theory. Figure 8(b) is constructed by averaging, for each size, the frequencies that correspond to the first elastic mode in elastic theory (e.g., the first 12 frequencies are averaged to obtain the lowest frequency point, the next 24 for the second point, and so on). The resulting frequency, divided by the value expected from elastic theory, is plotted as a function of wavelength. Note that all data points collapse on the same master curve irrespective of the box size L. Clearly, when the wavelength is lower than the self-averaging length, deviations from elastic theory become significant, whatever the size of the system. This estimate for the size of elastic inhomogeneity is therefore in fair agreement with those obtained in Secs. III and IV from the analysis of the linear response to an external load.

VI. DENSITY OF VIBRATIONAL STATES

The (normalized) density of vibrational states (DOS) of a 3D solid may be defined by $g(\omega)=(1/3N)\Sigma_{p=1}^{3N}\delta(\omega-\omega_p)$ with ω_p being the harmonic eigenfrequency corresponding to the mode number p. Hence, for small systems (of order of 10^3 beads) one can compute the complete DOS from the eigenfrequencies extracted by exact diagonalization of the dynamical matrix, just as we have done in Sec. V. Obviously, for systems containing about 10^5 particles, the number of modes one may compute is rather limited. From the 100 modes we have presented in Fig. 8, one estimates roughly $\omega_p^2\propto p^\alpha$ with $\alpha\approx 1$. Hence, the DOS increases approximately linearly, $g(\omega)\propto\omega^{2/\alpha-1}\approx\omega$, for small ω.

Following standard procedures,[22] we have instead obtained $g(\omega)$ by Fourier transformation of the velocity autocorrelation $\langle\underline{v}(t)\underline{v}(0)\rangle$. In contrast to the previous sections, we consider here configurations at finite, yet very low temperatures T. For the data presented in Fig. 9 we have used $T=10^{-4}$, which is three orders of magnitudes below the glass transition.[25] We start with quenched configurations at $T=0$, which we subject to a Maxwell velocity distribution. Following a thermalization phase of $\delta t=10^3\tau$, the velocity correlation function is sampled over $\delta t=100\tau$. Different temperatures have been checked, and we have verified that the DOS becomes temperature independent at low T (not shown). As can be seen from Fig. 9, our results become rapidly system-

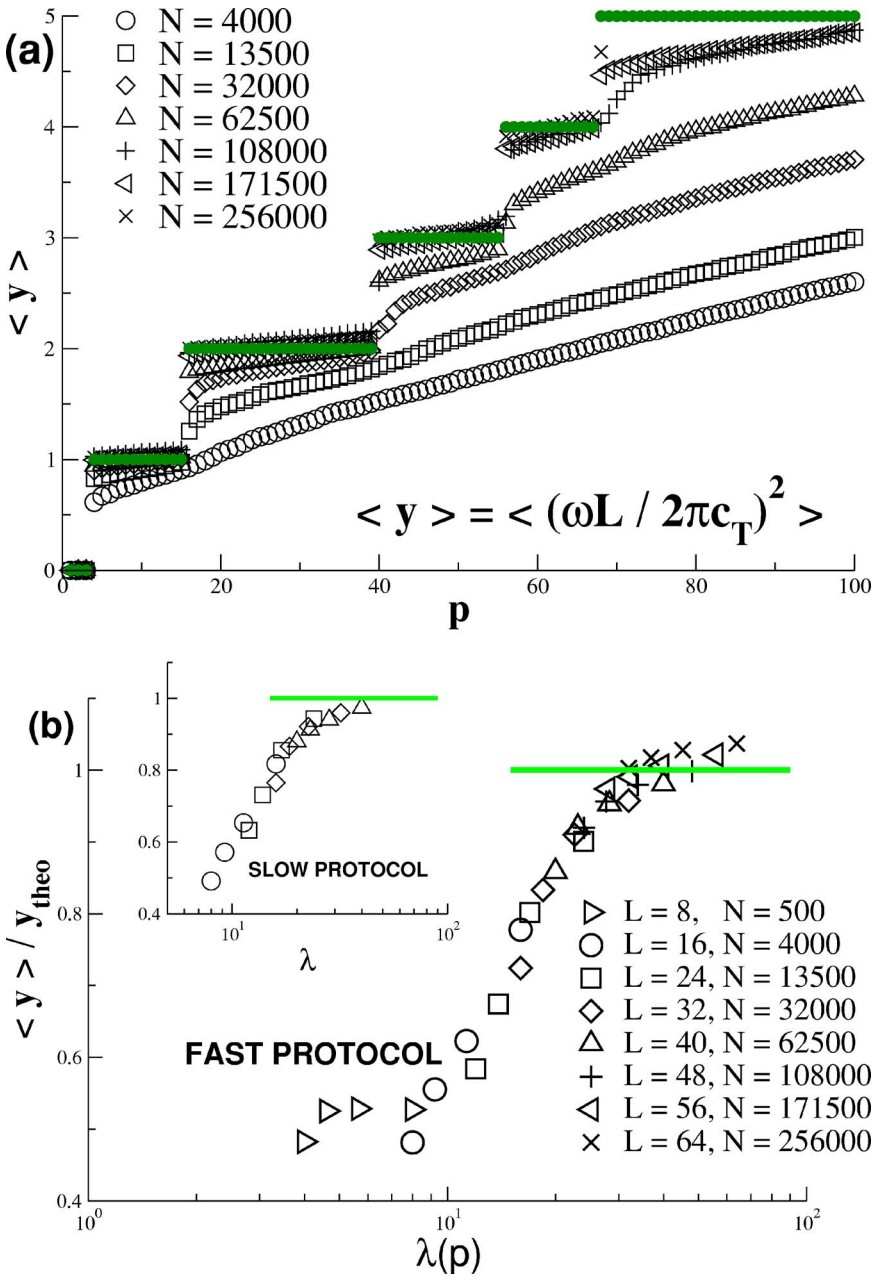

FIG. 8. (Color online) Rescaled and averaged equilibrium vibration modes $\langle y(p)\rangle$ in the low-frequency limit: (a) The first 100 modes are given as a function of the mode number p. The horizontal lines correspond to the results expected from macroscopic elasticity. Besides the obvious Goldstone modes ($p=1,2,3$), all frequencies are finite. Frequencies of small systems are systematically too low. (b) Plotting the same frequencies rescaled by the corresponding continuum theory prediction y_{theo} as a function of the expected wavelength $\lambda(p)=2\pi/\|\underline{k}\|$ yields a perfect data collapse for all L. The crossover to continuum behavior (horizontal line) takes place, as expected, at the self-averaging length $\lambda\simeq\xi$. The frequencies decrease systematically with smaller λ.

size independent for large frequencies $\omega\gg c_{T,L}2\pi/L$. (Only ω values corresponding to wave vectors $\underline{k}$ compatible with the box size are physically acceptable in the continuum limit. The corresponding finite size effects at low frequencies can be seen on the left-hand side of Fig. 9.)

In linear coordinates, $g(\omega)$ is roughly symmetric around its maximum at $\omega\approx 14.3$ and may be very crudely described as linear for small ω in agreement with the estimate from Fig. 8 described above and the dashed-dotted line indicated in the main panel of Fig. 9. Note that the maximum is slightly smaller than the Debye frequency $\omega_D=[18\rho\pi^2/(1/c_L^3+2/c_T^3)]^{1/3}\approx 18.3$ for our systems. (The Debye frequency is, in turn, smaller than the frequency $c_T 2\pi/\sigma\approx 26.4$ associated with a wavelength of monomer size.) The log-log plot presented in the main figure shows various frequency regimes. For very small frequencies, our data are in agreement with Debye's prediction $g_D(\omega)=3\omega^2/\omega_D^3$ (dashed line). The DOS increases more rapidly than with frequency up to $\omega_T=c_T 2\pi/\xi\approx 1.1$—corresponding to a wave vector given by the self-averaging length—where $g(\omega)$ has power-law slope of exponent 2 (bold line). This can be more clearly seen in the inset featuring the enigmatic Boson peak. Apparently, the width of this peak is well described by ω_T and the frequency $\omega_L\approx 2.3$ for the corresponding longitudinal wave. Hence, the Boson peak is fixed by the self-averaging length and marks the crossover between the continuum elastic behavior (dashed line) and the nonaffine displacement field regime, where $g(\omega)\propto\omega$ (dashed-dotted line), at larger ω and smaller wave length λ. Since continuum theory overestimates the frequencies for $\lambda\ll\xi$ (see

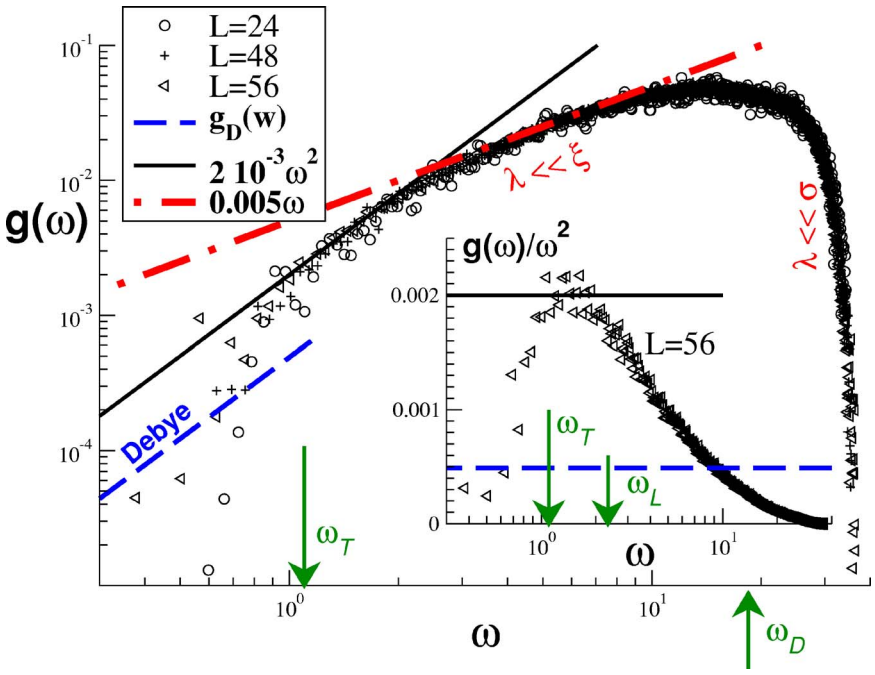

FIG. 9. (Color online) Density of states $g(\omega)$ for 3D amorphous systems of different system sizes L. The lines indicate three power-law slopes, the dashed one being the Debye prediction $g_D(\omega)$ calculated from the known sound velocities. The dashed-dotted linear relation corresponds to the nonaffine displacement field regime ($\lambda \ll \xi$). Also given are the characteristic frequencies $\omega_{L,T} = c_{L,T} 2\pi/\xi$ associated with the self-averaging length ξ and the Debye frequency $\omega_D \approx 18.3$. Larger frequencies correspond, in fact, to vibrations on very small scales, $\lambda \ll \sigma$. Inset: $g(\omega)/\omega^2$ vs ω for $L=56$. Note that ω_T and ω_L correctly describe the position and width of the boson peak.

also Fig. 8), this implies an excess of modes at smaller frequencies. Apparently, these modes are shifted to the edge of the nonaffine regime.

VII. CONCLUSION

We have investigated the approach of the continuum limit for elastic properties of 3D amorphous systems and compared our computational results to our previous work on similar 2D systems. The results are extremely similar in both cases and can be summarized as follows.

The elastic constants estimated using the Born formulas are not accurate even at zero temperature, therefore revealing the importance of the nonaffine component of the deformation field. This nonaffine deformation field, which mostly affects the shear response (as compared to compressibility), is correlated over intermediate distances of the order of 23 interatomic distances in our case. This correlation length is significantly smaller than in two dimensions, in agreement with the findings of Rossi *et al.*,[20] but implies that rather large samples should be used to discuss elastic or vibrational properties of 3D systems as well. By considering the Fourier transformation of solenoidal and longitudinal part of the nonaffine field, we have demonstrated (Fig. 6) that the 3D nonaffine field is mostly rotational in nature, in agreement with the visual impression of snapshots. The response to a δ-force perturbation allowed us to measure the self-averaging of the noisy response within a configuration. The stress fluctuations decay exponentially with distance from the source with a self-averaging length ξ similar to the correlation length of the nonaffine field. The nice agreement of all estimations of ξ is the first central result of this study.

Vibrational modes are obviously strongly affected by the existence of elastic heterogeneities and cannot be predicted using elastic theory if their wavelength is too small. From our scaling analysis [Fig. 8(b)], it appears that the frequencies are *smaller* than expected from continuum theory, therefore implying an excess of modes in the low-frequency region compared to the Debye prediction. This excess has been analyzed in Fig. 9 showing the density of vibrational states. It demonstrates that the Boson peak is located at the edge of the nonaffine displacement field and is thus merely a consequence of the inapplicability of the continuum theory at $\lambda \ll \xi$. That both position and width of the peak are given by the self-averaging length ξ is our second central result.

The focus of this work has been primarily on the *linear elastic* behavior of amorphous solids. Our preliminary study of larger (uniaxial) deformations that go beyond the elastic limit indicates that plastic events are rather localized individual events characterized by a very low participation ratio. In the recent work,[18] de Pablo and co-workers pointed out the possibility of *regions of negative shear modulus* in quenched amorphous systems—such regions being stabilized by the "normal" material in which they are embedded. The typical size of these regions is much smaller than the size for elastic inhomogeneities discussed in this work, implying they are more likely to be linked to elementary rearrangements taking place at the onset of plastic deformation, which usually imply small numbers of particles,[9–12,28] or even localization along a shear band.[13,14] Such a difference in elastic and plastic deformations was also observed for 2D systems in Ref. 9.

The general picture that emerges is, therefore, that of a hierarchy of length scales. Disorder at the level of a few atomic distances can be interpreted as implying the existence of regions with negative moduli, which will give rise to plastic yield. On a larger scale, this disorder gives rise to strong nonaffine displacement fields in elementary deformations. Finally, convergence to standard continuum properties is

obtained over length scales larger than the self-averaging length. In our analysis, carried out for a typical liquid state density and at zero temperature, ξ is found to be large, but finite. In analogy with what is found in two dimensions, we expect it to decrease with increasing density and possibly to diverge as the density is lowered and the system loses mechanical stability, as suggested in Ref. 19.

ACKNOWLEDGMENTS

During the course of this work, we had valuable discussions with A. Lemaître, C. Maloney, J. de Pablo, B. Schnell, and D. Vandembroucq. Computational support by IDRIS/France is acknowledged. F.L. was supported by the Emergence 2002 Program of the Conseil Regional Rhônes-Alpes (France).

*Email: fleonfor@lpmcn.univ-lyon1.fr

[1] J. P. Wittmer, A. Tanguy, J.-L. Barrat, and L. Lewis, Europhys. Lett. **57**, 423 (2002).
[2] A. Tanguy, J. P. Wittmer, F. Leonforte, and J.-L. Barrat, Phys. Rev. B **66**, 174205 (2002).
[3] F. Leonforte, A. Tanguy, J. P. Wittmer, and J.-L. Barrat Phys. Rev. B **70**, 014203 (2004).
[4] S. Alexander, Phys. Rep. **296**, 65 (1998).
[5] L. D. Landau and E. M. Lifshitz, *Theory of Elasticity* (Butterworth-Heinemann, London, 1995).
[6] E. Duval and A. Mermet, Phys. Rev. B **58**, 8159 (1998).
[7] V. A. Luchnikov, N. N. Medvedev, Y. I. Naberukhin, and V. N. Novikov, Phys. Rev. B **51**, 15569 (1995).
[8] G. Masciovecchio *et al.* (unpublished).
[9] C. Maloney and A. Lemaître, Phys. Rev. Lett. **93**, 016001 (2004); Phys. Rev. Lett. **93**, 195501 (2004); A. Lemaître and C. Maloney, J. Stat. Phys. (to be published).
[10] M. L. Falk and J. S. Langer, Phys. Rev. E **57**, 7192 (1998); Phys. Rev. B **60**, 7062 (1999).
[11] J. Y. Cavaillé, J. Perez, and G. P. Johari, Phys. Rev. B **39**, 2411 (1989).
[12] A. Kabla and G. Debrégeas, Phys. Rev. Lett. **90**, 258303-1 (2003).
[13] J. C. Baret, D. Vandembroucq, and S. Roux, Phys. Rev. Lett. **89**, 195506 (2002).
[14] G. Picard, A. Ajdari, F. Lequeux, and L. Bocquet, Phys. Rev. E **71**, 010501(R) (2005).
[15] M. D. Ediger, Annu. Rev. Phys. Chem. **51**, 99 (2000).
[16] I. Goldhirsch and C. Goldenberg, Eur. Phys. J. E **9**, 245 (2002).
[17] F. Leonforte *et al.* (unpublished).
[18] K. Yoshimoto, T. S. Jain, K. Van Workum, P. F. Nealey, and J. J. de Pablo, Phys. Rev. Lett. **93**, 175501 (2004).
[19] M. Wyart, L. E. Silbert, S. R. Nagel, and T. A. Witten, Phys. Rev. E **72**, 051306 (2005); L. E. Silbert, A. J. Liu, and S. R. Nagel, Phys. Rev. Lett. **95**, 098301 (2005); M. Wyart, S. R. Nagel, and T. A. Witten, Europhys. Lett. **72**, 486 (2005).
[20] B. Rossi, G. Viliani, E. Duval, L. Angelani, and W. Garber, Europhys. Lett. **71**, 256 (2005).
[21] V. A. Luchnikov, N. N. Medvedev, Yu. I. Naberukhin, and H. R. Schober, Phys. Rev. B **62**, 3181 (2000); H. R. Schober and C. Oligschleger, *ibid.* **53**, 11469 (1996); H. R. Schober and B. B. Laird, *ibid.* **44**, 6746 (1991).
[22] S. V. Meshkov, Phys. Rev. B **55**, 12113 (1997).
[23] P. B. Allen, W. Garber, and L. Angelani, cond-mat/0307435 (unpublished).
[24] J.-L. Barrat and J.-P. Hansen, J. Phys. (Paris) **47**, 1547 (1987); P. N. Pusey, *ibid.* **48**, 709 (1987).
[25] Additional information on technical details may be found in F. Leonforte, Ph.D. thesis, Université Claude Bernard, Lyon I (2005).
[26] The jumps in the plateau value at small strains (below 10^{-6}) in Fig. 3, specifically for the slow protocol, are due to numerical inaccuracies.
[27] The more gradual decay of the participation ratio, in the fast protocol case (Fig. 3), is due to ensemble averaging. It describes the probability that no jump has occurred for smaller ϵ values, and it is thus related to the *distribution* of the plastic thresholds ϵ_p from one configuration to the other. For each individual configuration, the decay of the participation ratio is more sudden and can be compared to the averaged decay in the slow protocol case, where the distribution of ϵ_p is narrower. This is, in fact, the main difference observed between the two quench protocols: the plastic threshold ϵ_p is well defined in the slow quench protocol case, but it is distributed over more that one decade for the fast quench protocol. Unfortunately, our configuration ensemble are not large enough to allow a precise computation of this distribution.
[28] D. Malandro and D. J. Lacks, J. Chem. Phys. **110**, 4593 (1999).
[29] Free software developed by R. Lehoucq, K. Maschhoff, D. Sorensen, and C. Yang, Rice University. See http://www.caam.rice.edu/software/ARPACK/
[30] The rescaling eliminates trivial dependencies on system size and sound velocities, which are anyway expected from continuum theory. The rescaled frequencies are averaged over the ensemble of available configurations. Note that differences between the eigenfrequencies of different configurations of the ensemble are weak, however, even for small system sizes.